Angewandte Chemie
Eine Zeitschrift der Gesellschaft Deutscher Chemiker

Supporting Information

Microtubular Self-Assembly of Covalent Organic Frameworks

*Bappaditya Gole, Vladimir Stepanenko, Sabrina Rager, Matthias Grüne, Dana D. Medina, Thomas Bein, Frank Würthner, and Florian Beuerle**

anie_201708526_sm_miscellaneous_information.pdf

Contents:

1 General Information

Solvents and reagents were purchased from commercial sources and used without further purification, unless otherwise mentioned. *2,5-Diethylhexyl-3,6-dithiophen-2-ylpyrrolo[3,4-c]pyrrole-1,4-dione* (**1**),[S1] tetraphenylporphyrin[S2] and 5,10,15,20-tetrakis(4-aminophenyl)-porphyrin (**TAPP**)[S2] were prepared according to previously reported procedures. Spectroscopic measurements were conducted under ambient conditions using dry solvents. Nuclear magnetic resonance (NMR) spectra were recorded on a Bruker Avance III HD (400 MHz) spectrometer. Chemical shifts are reported in parts per million (ppm) with respect to residual $CHCl_3$ (0 ppm for ^1H and 77 ppm for ^{13}C) as the internal standard. Signal multiplicities are denoted as s (singlet), d (doublet), t (triplet), and m (multiplet). Processing of the raw data was performed by using the program Topspin 3.0. Solid state ^{13}C cross-polarization magic-angle spinning (CP-MAS) NMR spectra were measured on a Bruker Avance III HD 600 MHz NMR spectrometer with a spinning rate of 17000 Hz and a contact time of 2 ms and on a Bruker DSX 400 MHz spectrometer with a spinning rate of 13500 Hz and a contact time of 2 ms. Mass spectroscopic analyses (MALDI) were carried out on an Autoflex II BRUKER spectrometer using trans-2-(3-(4-t-butylphenyl)-2-methyl-2-propenylidene) malononitrile (DCTB) as matrix. Elemental analyses (%) were carried out on an Elementar CHNS 932 analyzer. Fourier transform infrared (FT-IR) spectroscopic analysis was performed on a Jasco FT/IR-430 Spectrometer. Thermogravimetric analysis (TGA) measurements were performed on a Netzsch Jupiter ST 449 C instrument equipped with a Netzsch TASC 414/4 controller. The samples were heated from room temperature to 900 °C under nitrogen atmosphere at a heating rate of 1 °C/min. Powder X-ray diffraction (PXRD) measurements were carried out in reflection mode on a Bruker D8 Discover diffractometer with Ni-filtered Kα-radiation (λ = 1.54060 Å) and a position-sensitive detector (LynxEye). The PXRD measurements of resulting COF materials were carried out on a silicon wafer and by applying low scan speed and small angle increments. Scanning Electron Microscopy (SEM) images were recorded using a Zeiss Ultra Plus field emission scanning electron microscope equipped with GEMINI e-Beam column operated at 1 ─ 1.5 kV with an aperture size set to 30 μm to avoid excessive charging and radiation damage of the areas imaged. Focused ion beam (FIB) experiments were carried out in a Dual-Beam System incorporating both FIB and SEM using FEI Helios Nanolab. The FIB milling was performed using a 30 kV Ga-ion beam with beam currents ranging from 90 to 170 pA. A protective platinum film (30 nm thick) was deposited on the sample prior to milling. SEM images were obtained using low acceleration voltages (5 kV) and low beam currents (0.17 nA) to limit beam damage. Atomic Force Microscopy (AFM) measurements were performed at ambient conditions with a Bruker AXS MultiMode^{TM} Nanoscope IV System in tapping mode. Silicon cantilevers (OMCL-AC160TS, Olympus) with a resonance frequency of ~ 300 kHz and spring constant of ~ 42 Nm^{-1} were used.

2 Synthetic Procedures

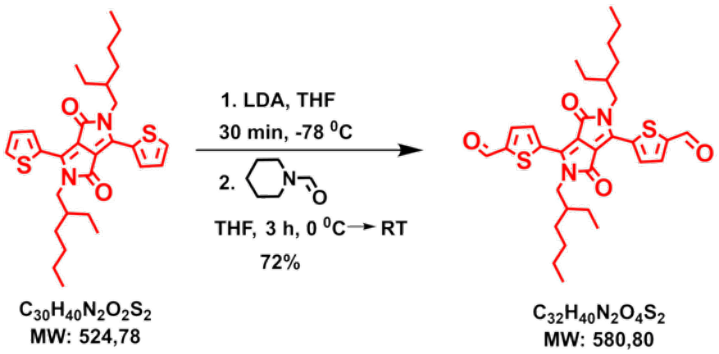

5,5'-(2,5-bis(2-ethylhexyl)-3,6-dioxo-2,3,5,6-tetrahydropyrrolo[3,4-c]pyrrole-1,4-diyl)dithiophene-2-carbaldehyde (DPP-1): **DPP-1** was prepared following a slightly modified literature procedure[S3-S5] resulting in increased isolated yields. In a three necked round bottom flask, **1**[S1] (819 mg, 1.56 mmol, 1 eq) was dissolved in anhydrous THF (80 mL). At −78 °C, freshly prepared lithium diisopropylamide (LDA) (0.32 M, 12.5 mL, 2.5 eq) was added dropwise under N_2 and constant stirring. The mixture was stirred at the same temperature for another 30 minutes. Afterwards, the solution was slowly warmed up to 0 °C. Subsequently, 1-formylpiperidine (0.43 mL, 3.9 mmol, 2.5 eq) was added dropwise to the solution. The reaction was stirred at room temperature for another three hours. Finally, the reaction mixture was poured into 0.3 M aqueous HCl (150 mL) and stirred vigorously for ten minutes. The organic portion was extracted with $CHCl_3$ (5 × 50 mL). The combined phases were washed with a saturated aqueous solution of $NaHCO_3$ (3 × 30 mL) and brine solution, dried over Na_2SO_4 and finally concentrated under reduced pressure to get the crude product. The crude product was purified by silica gel column chromatography using $CHCl_3$/*n*-hexane (1:1) as eluent to obtain **DPP-1** as a dark purple solid (650 mg, 1.12 mmol, 72%). **^{1}H NMR** (400 MHz, $CDCl_3$, rt): δ = 10.03 (s, 2H), 9.05 (d, *J* = 4.16 Hz, 2H), 7.88 (d, *J* = 4.23 Hz, 2H), 4.07 (m, 4H), 1.85 (m, 2H), 1.38 (m, 16H), 0.91 (m, 12H) ppm. **MS** (MALDI-TOF, DCTB): *m/z* = 580.262 $[M]^+$.

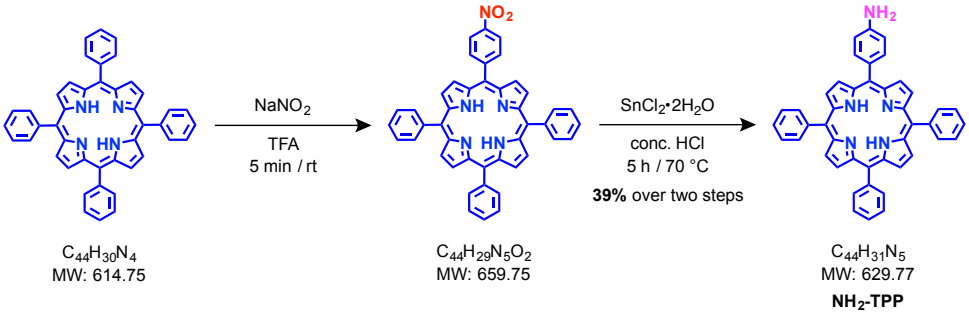

5-(4-aminophenyl)-10,15,20-triphenylporphyrin (NH_2-TPP): The title compound was prepared using a modified literature procedure.[S6-S7] To a solution of tetraphenylporphyrin[2] (1.5 g, 2.44 mmol, 1 eq) in trifluroacetic acid (70 mL), $NaNO_2$ (303.6 mg, 4.4 mmol, 1.8 eq) was added in one portion. After stirring the solution for five minutes at room temperature, the whole mixture was poured into water (300 mL). Finally, the organic layer was extracted with CH_2Cl_2 (5 × 50 mL). The combined organic phases were washed with a saturated aqueous

solution of $NaHCO_3$ (3 × 30 mL), dried over Na_2SO_4 and finally concentrated under vacuum to get the crude nitration product. The crude product was used without further purification for the next step.

The crude product was dissolved in concentrated HCl (70 mL) under constant stirring and heated to 70 °C for one hour. After cooling down again to room temperature, $SnCl_2 \cdot 2H_2O$ (4.4 g, 19.5 mmol, 8 eq) was added in small portions under constant stirring. The reaction mixture was again heated to 70 °C with an overhead refluxing condenser for another five hours. Subsequently, the mixture was poured into an ice-water bath. The aqueous solution was neutralized by addition of aqueous ammonia until the pH reached 8. Afterwards, the aqueous solution was extracted with CH_2Cl_2 (5 × 50 mL). The combined organic phases were dried over anhydrous Na_2SO_4 and finally concentrated under vacuum. The obtained residue was purified by column chromatography using neutral alumina as stationary phase and CH_2Cl_2 as eluent to obtain **NH_2-TPP** (600 mg, 0.95 mmol, 39% over two steps) as a dark purple crystalline solid. **^{1}H NMR** (400 MHz, DMSO-d_6, rt): δ = 8.98 (d, J = 4.5 Hz, 2H), 8.81 (m, 6H), 8.23 (m, 6H), 7.85 (m, 11H), 7.0 (d, J = 8.4 Hz, 2H), 5.62 (s, 2H), -2.86 (s, 2H) ppm. **MS** (MALDI-TOF, DCTB): m/z = 629.236 $[M]^+$.

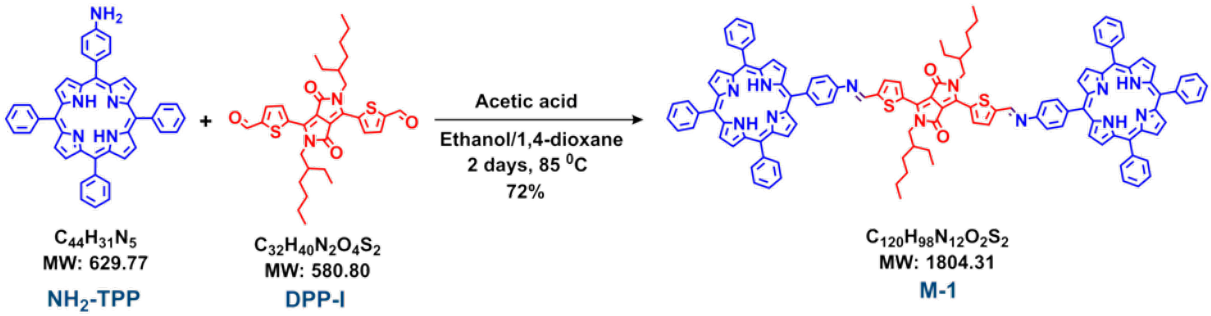

Model compound M-1: **NH_2-TPP** (55.42 mg, 0.088 mmol, 2.2 eq) and **DPP-1** (23.23 mg, 0.04 mmol, 1 eq) were dissolved in a mixture of EtOH (10 ml), 1,4-dioxane (10 ml) and AcOH (0.05 mL). The reaction mixture was heated to 85 °C under constant stirring in the presence of molecular sieves 4Å for two days. After cooling down to room temperature, the solvents were completely removed under vacuum and the obtained residue was dissolved in $CHCl_3$ and filtrated in order to remove the molecular sieves. The filtrate was evaporated to dryness to yield a dark purple solid as the crude product. Final purification was performed by recycling gel permeation chromatography using $CHCl_3$ as the eluent to obtain pure model compound **M-1** (52 mg, 28.8 µmol, 72%) as a dark purple solid. **^{1}H NMR** (400 MHz, $CDCl_3$, rt): δ = 9.18 (d, J = 4.1 Hz, 2H), 9.02 (s, 2H), 8.92 (m, 16H), 8.29 (d, J = 8.5 Hz, 4H), 8.25 (m, 12H), 7.80 (m, 20H), 7.70 (d, J = 8.4 Hz, 4H), 4.26 (m, 4H), 2.05 (m, 2H), 1.48 (m, 16H), 1.02 (m, 12H), -2.75 (s, 2H) ppm. **^{13}C NMR** (100 MHz, $CDCl_3$, rt): δ = 161.76, 152.26, 150.18, 147.45, 142.16, 140.90, 140.55, 136.56, 135.58, 134.58, 133.24, 132.81, 127.77, 126.73, 120.26, 119.67, 119.44, 110.02, 77.23, 46.26, 39.37, 30.29, 29.73, 28.51, 23.68, 23.18, 14.19, 10.60 ppm. **MS** (MALDI-TOF, DCTB): m/z = 1803.295 $[M]^+$. **Elemental analysis** (%) calculated for $C_{120}H_{98}N_{12}O_2S_2$: C 79.88, H 5.47, N 9.32, S 3.55; found: C 79.59, H 5.48, N 9.12, S 3.34.

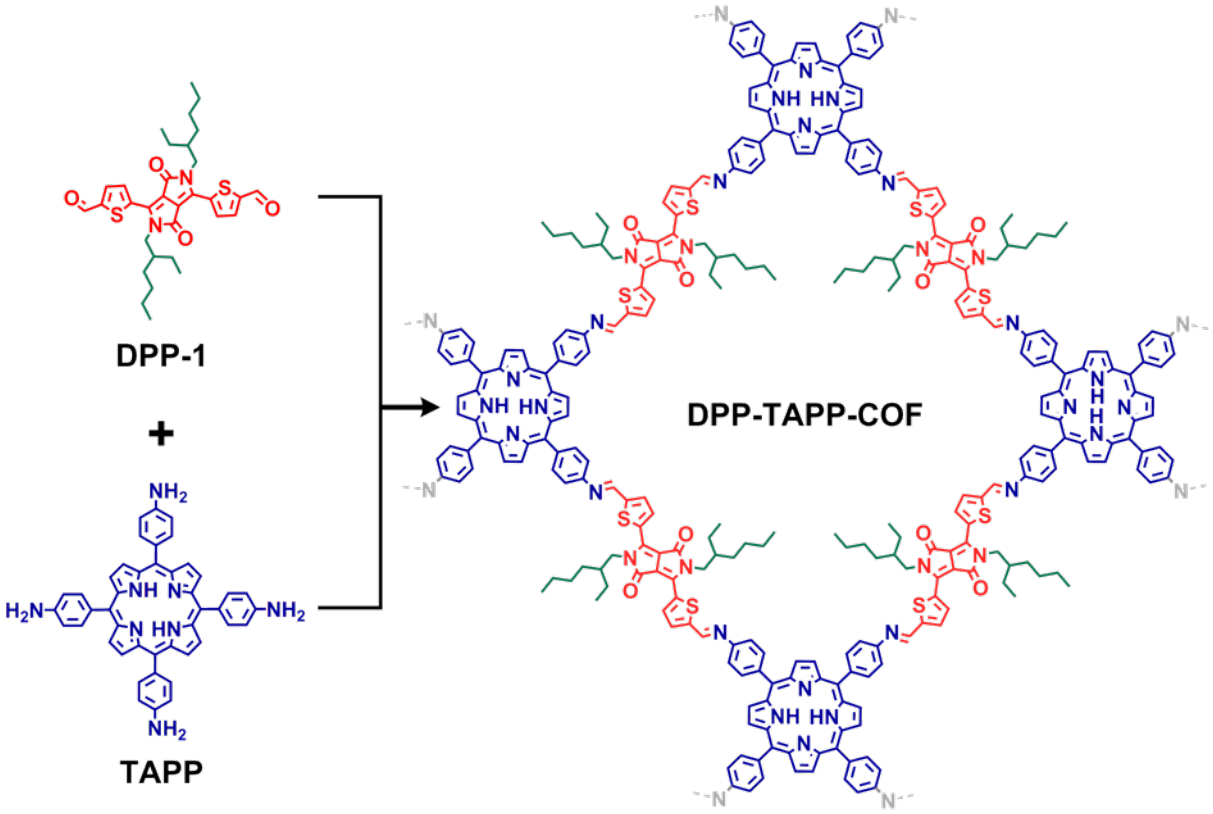

Synthesis of DPP-TAPP-COF: A pyrex tube with a screw cap was charged with 5,10,15,20-tetrakis(4-aminophenyl)porphyrin (**TAPP**)[S2] (6.75 mg, 0.01 mmol, 1 eq) and **DPP-1** (11.61 mg, 0.02 mmol, 2 eq). To that mixture, *n*-butanol (3 mL), mesitylene (1 mL) and aqueous acetic (0.1 ml of 6.0 M aqueous solution) were added. The reaction mixture was sonicated for five minutes in order to homogeneously disperse all reactants. The reaction vessel was sealed with a screw cap and heated at 120 °C for five days. The obtained dark precipitate was collected by filtration through a sintered funnel and washed with dry THF and acetone for three times. The powder obtained was solvent exchanged with ethanol and acetone for three times each and subsequently dried under high vacuum for another four hours to obtain **DPP-TAPP-COF** as dark powder (9.35 mg, 53%). FT-IR (transmittance/cm^{-1}): 1667, 1608, 1581, 1560, 1514, 1464, 1457, 1399, 1349, 1222, 1197, 1095, 1019, 966, 796, 733, 711, 624. Elemental analysis (%): calculated for $C_{108}H_{106}N_{12}O_4S_4$: C 73.52, H 6.06, N 9.53, S 7.27; found: C 72.37, H 6.01, N 9.35, S 6.24.

Synthesis of COF at different time intervals: The reaction mixture was distributed to several pyrex tubes and individual samples were removed from the oven after specified time intervals. After cooling to room temperature, precipitates were collected and dried in a similar fashion as described before. The obtained materials were further characterized by PXRD (Figure S16), SEM (Figure S17), IR (Figures S8 and S19) and solid-state NMR (Figure S20).

Synthesis using different solvents: Different solvents and their combinations were investigated for COF synthesis as summarized in Table S1. All reactions were carried out using 0.02 mmol of **DPP-1** and 0.01 mmol of **TAPP**. The obtained precipitates were analyzed by PXRD (see Figure S21).

Table S1. Solvent and catalyst screening for DPP-TAPP-COF synthesis

Entry	Solvents				Temp.	Time	Remarks
	n-butanol	mesitylene	*o*-DCB	AcOH (6 M)			
1	**3 mL**	**1 mL**	**-**	**0.1 mL**	**120 °C**	**5 days**	**Crystalline**
2	2 mL	2 mL	-	0.1 mL	120 °C	5 days	Amorphous
3	2 mL	-	2 mL	0.1 mL	120 °C	5 days	Amorphous
4	3 mL	-	2 mL	0.1 mL	120 °C	5 days	Minor crystalline
5	4 mL	-	-	0.1 mL	120 °C	5 days	No reaction
6	3 mL	1 mL	-	0.2 mL	120 °C	5 days	Amorphous
7	1.5 mL	0.5 mL	-	0.1 mL	120 °C	5 days	Minor crystalline
8	4.5 mL	1.5 mL	-	0.1 mL	120 °C	5 days	Amorphous
9	3 mL	1 mL	-	-	120 °C	5 days	Amorphous
10	4.5 mL	1.5 mL	-	-	120 °C	5 days	Amorphous
11	9 mL	3 mL	-	0.1 mL 12 M	120 °C	5 days	Amorphous

3 Analytical Data

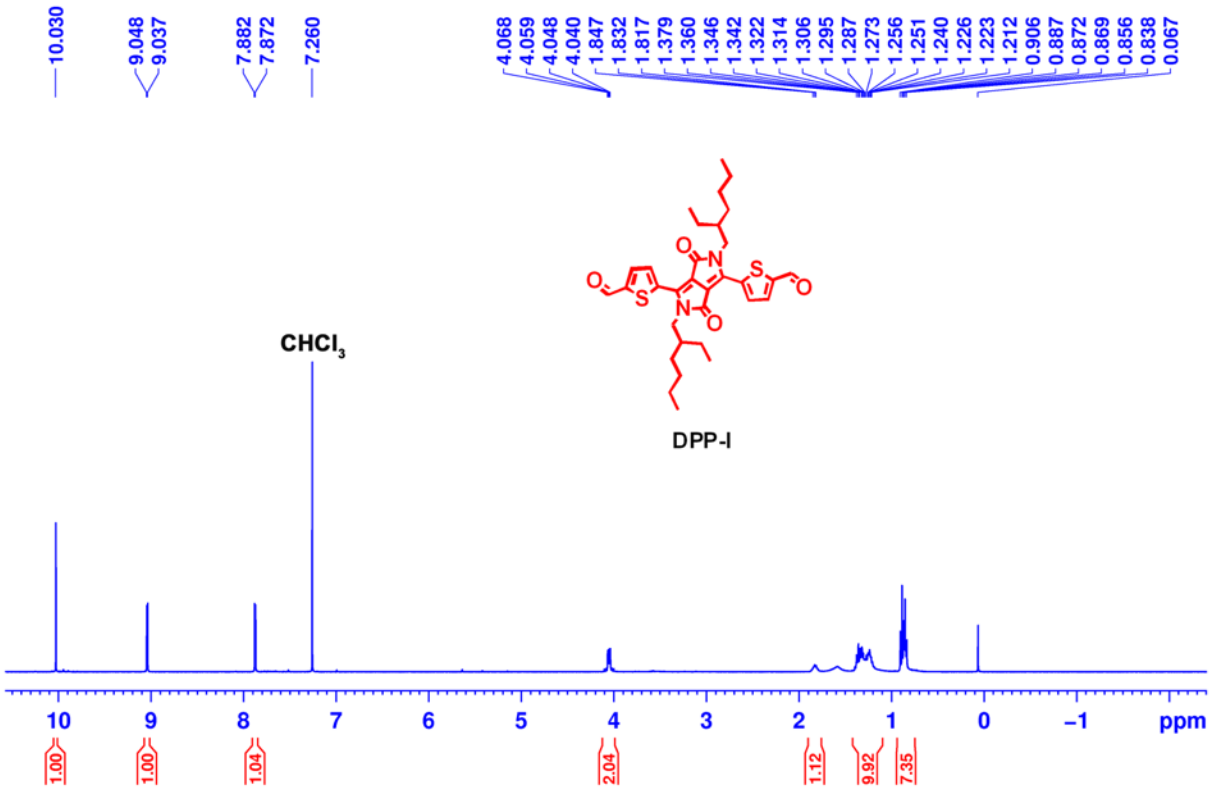

Figure S1. ^{1}H-NMR (400 MHz, $CDCl_3$, rt) spectrum of **DPP-1**.

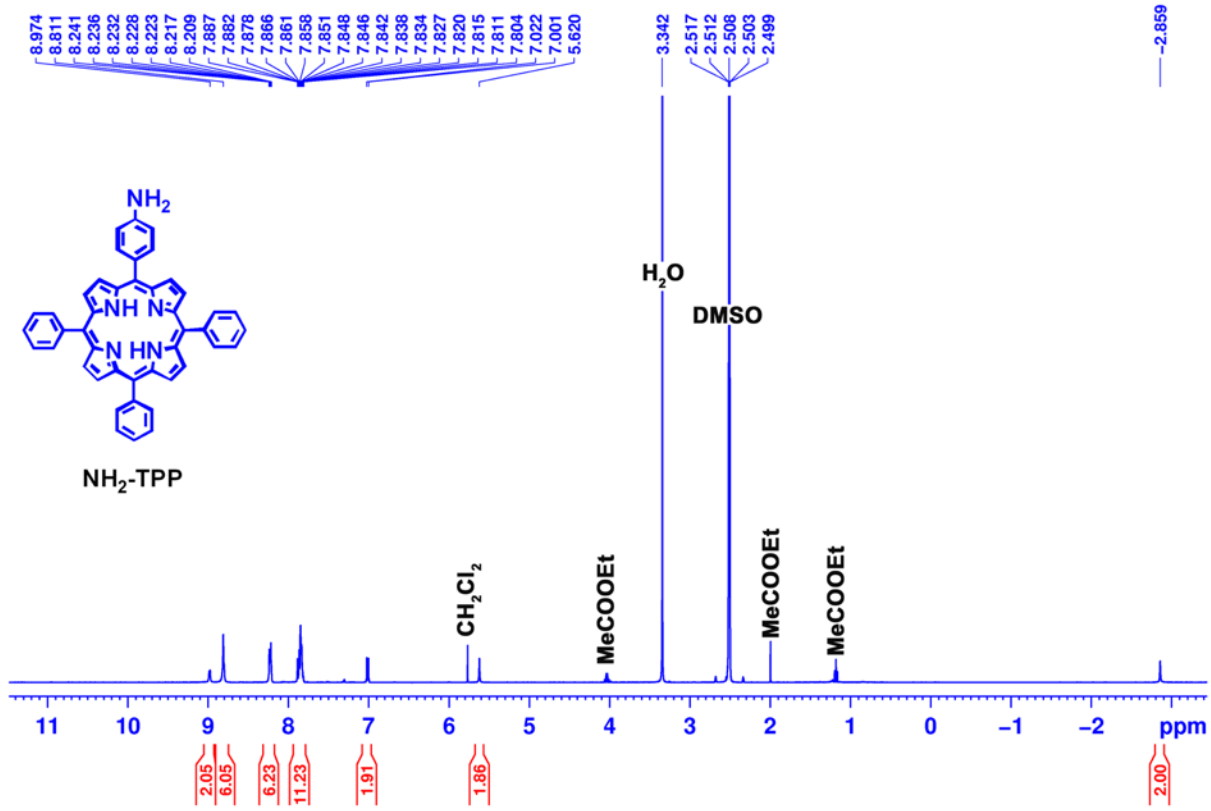

Figure S2. ^{1}H-NMR (400 MHz, $CDCl_3$, rt) spectrum of **NH_2-TPP**.

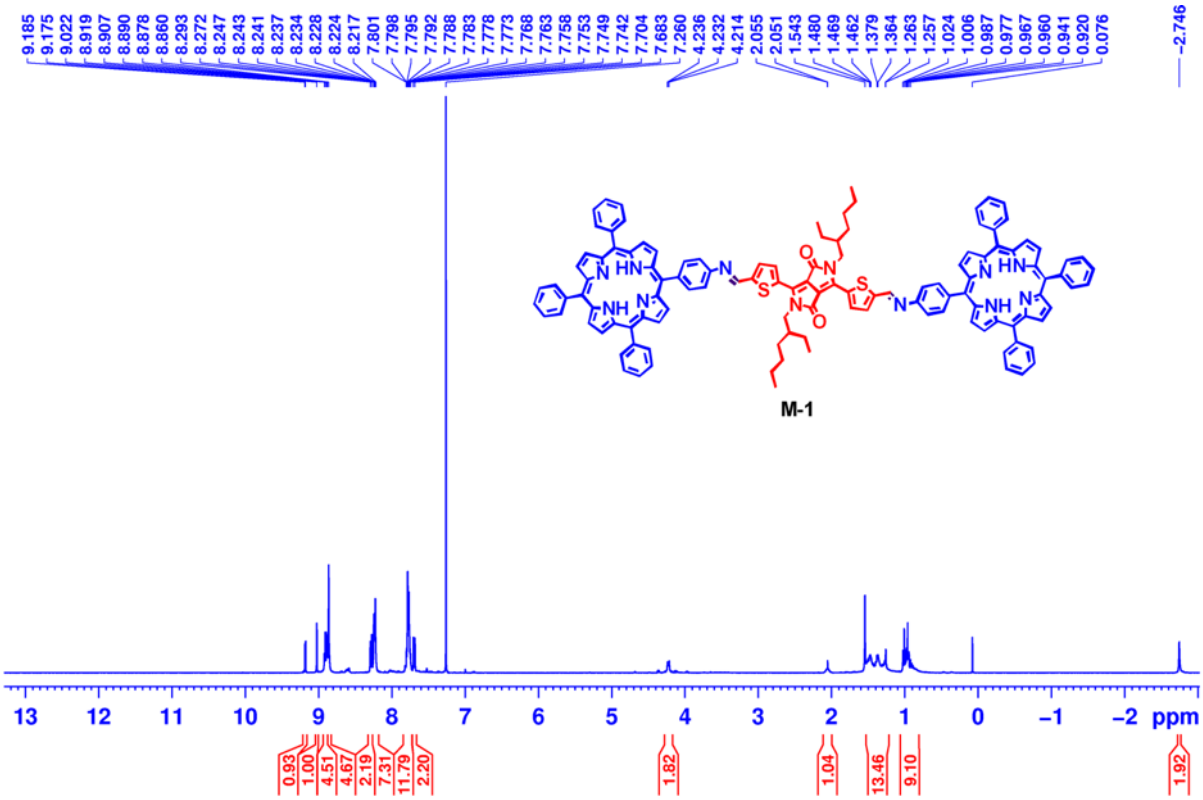

Figure S3. ^{1}H-NMR (400 MHz, $CDCl_3$, rt) spectrum of **M-1**.

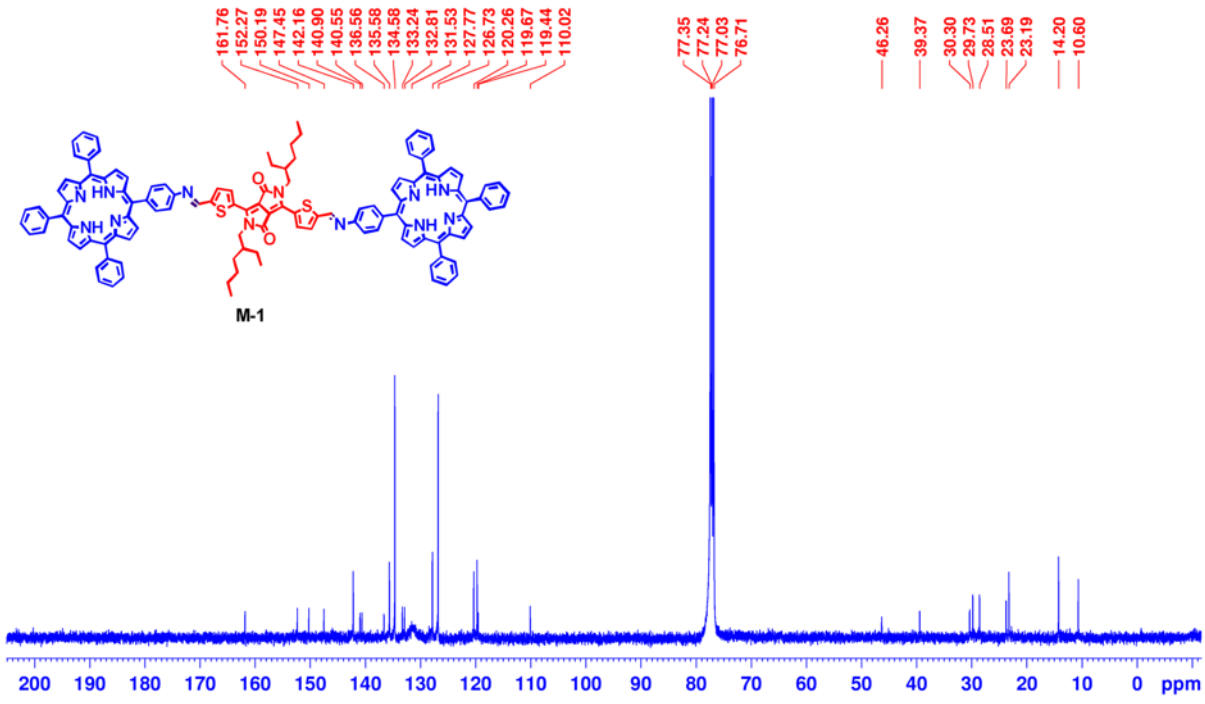

Figure S4. ^{13}C-NMR (100 MHz, $CDCl_3$, rt) spectrum of **M-1**.

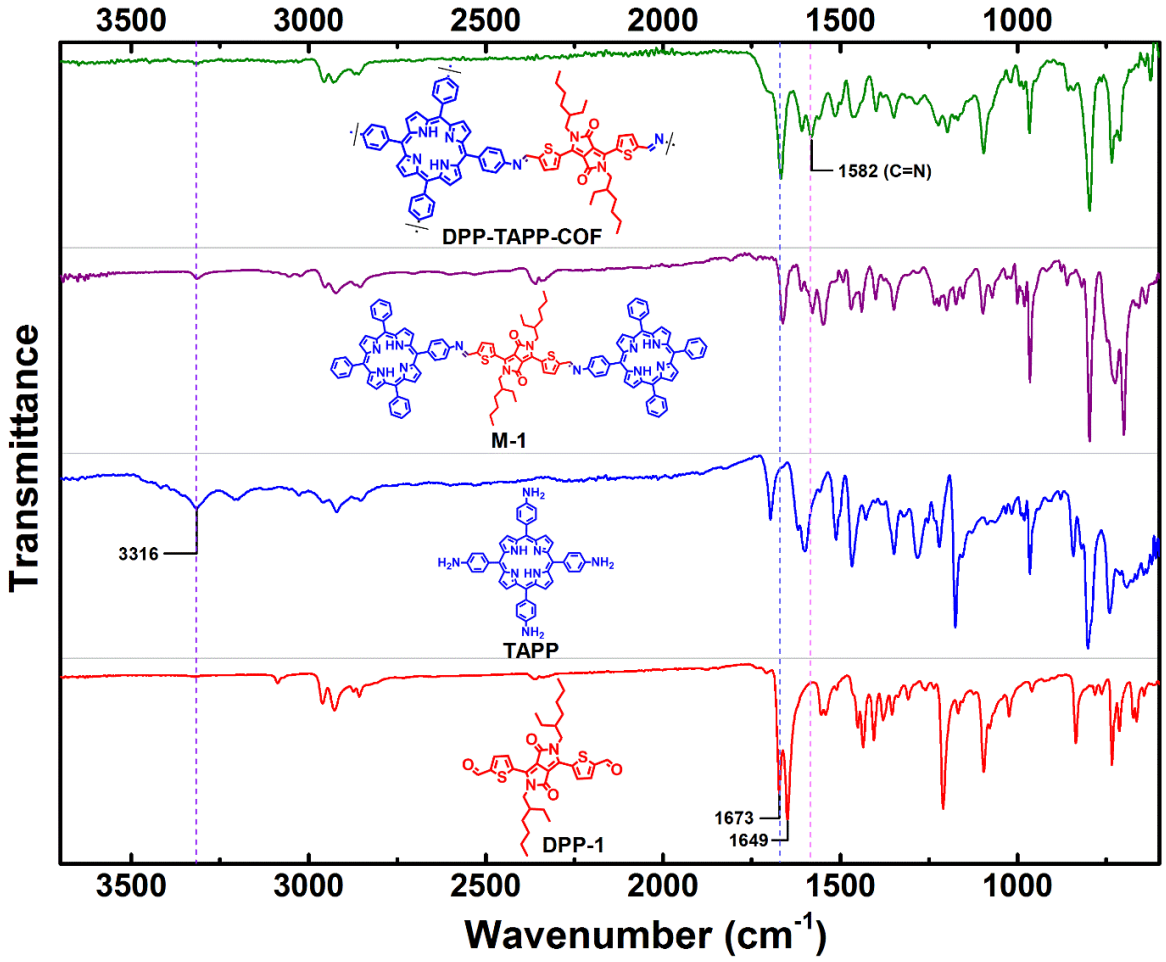

Figure S5. FTIR spectra for **DPP-TAPP-COF** (top) in comparison with model compound **M-1** and corresponding monomers **DPP-1** and **TAPP**.

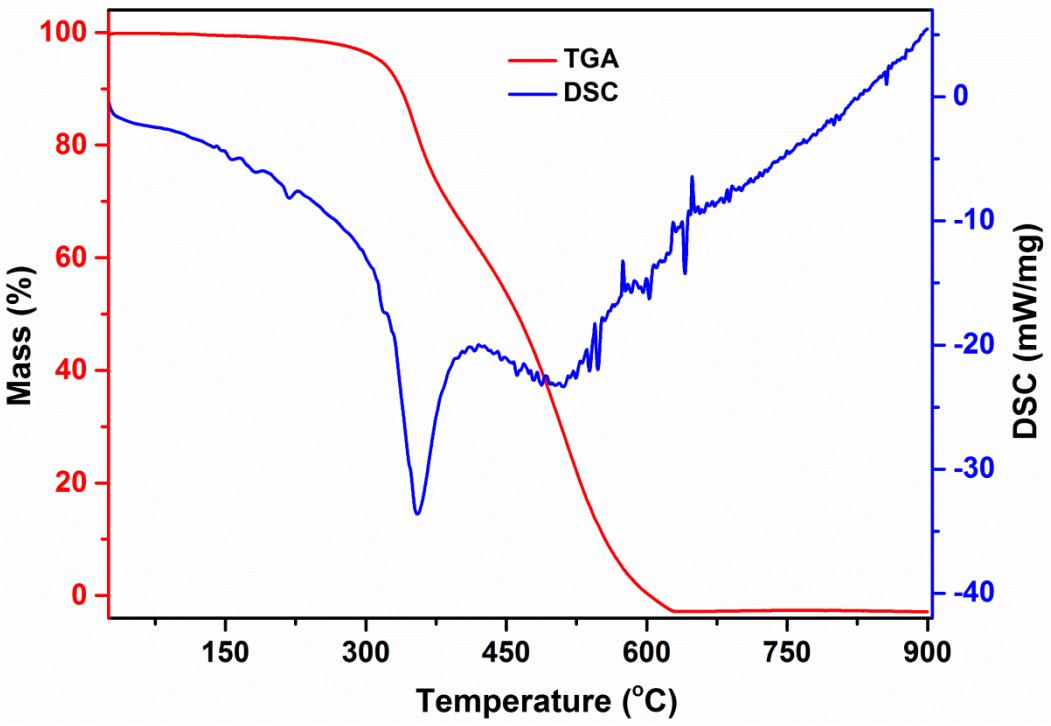

Figure S6. Thermogravimetric (TG) and DSC analyses for **DPP-TAPP-COF** under N_2.

4 PXRD Analysis

Based on the precursor geometries and linking groups the COF structure was constructed; the simulations were carried out with the visualization environment of *Materials Studio software 4.4*. Firstly, an optimized geometry of the two-dimensional COF layers was obtained by using the forcite module. Subsequently, the COF repeating unit was inserted into the unit cell of the appropriate size and symmetry. The geometry of the **DPP-TAPP-COF** layer was optimized in the unit cell using the Dreiding forcefield and the QEq correction for weak interactions. Moreover, DFTB+ calculations were carried out by using the mio Slater-Koster library. The X-ray diffraction pattern for the simulated structure was obtained by using the Reflex package in the *Material Studio software*. Furthermore, Pawley refinement according to the experimental PXRD provided the final unit cell parameters. The refinement parameters R_p and R_{wp} are 2.86% and 3.82%, respectively.

Table S2. Refined crystal data.

Space group	C2/m
Crystal system	monoclinic
Chemical formula	$C_{216}H_{208}N_{24}O_8S_8$
Unit cell dimension	a = 45.29 Å b = 48.91 Å c = 3.9 Å α = γ = 90.00° β = 74.37°
Cell Volume	8358.91 $Å^3$

Table S3. Fractional atomic coordinates.

Atom	x/a	y/b	z/c
C1	444.701	-144.969	-0.54591
C2	448.515	-141.184	-0.51142
C3	447.624	-144.040	-0.52372
C4	443.798	-147.746	-0.56131
C5	440.929	-148.605	-0.63098
C6	442.330	-142.896	-0.54544
C7	442.895	-140.599	-0.77182
C8	440.620	-138.667	-0.76283
C9	437.681	-138.956	-0.52548
C10	437.108	-141.254	-0.29726
C11	439.384	-143.184	-0.30948
N12	435.518	-136.919	-0.52608
C13	430.646	-134.899	-0.34784
S14	431.978	-132.151	-0.62488
C15	428.526	-130.390	-0.47971
C16	426.409	-131.982	-0.22762
C17	427.589	-134.513	-0.15593

C18	427.756	-127.680	-0.57356
N19	429.538	-125.914	-0.82356
C20	427.936	-123.465	-0.85131
C21	424.982	-126.309	-0.41864
O22	428.949	-121.684	-107.609
C23	432.691	-137.142	-0.33762
C24	0.32384	0.73441	-0.08180
C25	0.35217	0.74910	-0.02123
C26	0.37928	0.72939	-0.12787
C27	0.40918	0.74120	-0.08992
C28	0.43427	0.71977	-0.15575
C29	0.46387	0.73150	-0.10998
C30	0.35841	0.77637	-0.22330
C31	0.36953	0.79953	-0.03393
H32	447.139	-139.369	-0.52539
H33	439.165	-147.292	-0.68969
H34	445.132	-140.392	-0.96755
H35	441.090	-136.907	-0.94432
H36	434.866	-141.522	-0.10464
H37	438.897	-144.916	-0.12352
H38	424.080	-131.242	-0.09684
H39	426.286	-136.027	0.03179
H40	431.751	-138.948	-0.16736
H41	0.32100	0.73987	-0.34617
H42	0.32713	0.71197	-0.08361
H43	0.34770	0.75329	0.26575
H44	0.38226	0.72259	-0.40502
H45	0.37380	0.71069	0.03740
H46	0.40585	0.74969	0.18014
H47	0.41652	0.75844	-0.27629
H48	0.43799	0.71113	-0.42614
H49	0.42674	0.70250	0.03057
H50	0.47465	0.74541	-0.33000
H51	0.48031	0.71504	-0.10042
H52	0.45984	0.74331	0.13897
H53	0.33713	0.78324	-0.28575
H54	0.37568	0.77273	-0.47787
H55	0.37623	0.81700	-0.21534
H56	0.38957	0.79380	0.05893
H57	0.35137	0.80670	0.19446
N58	0.50000	0.54318	0.50000
N59	0.45465	0.50000	0.47462

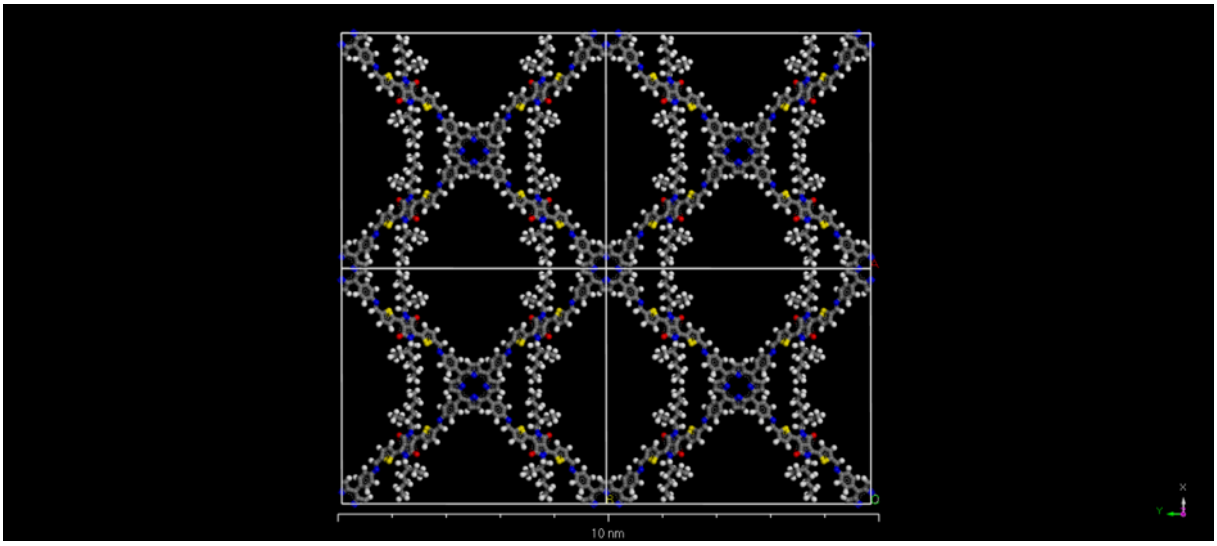

Figure S7. Simulation of **DPP-TAPP-COF** unit cell calculated in an eclipsed arrangement in the *C2/m* space group.

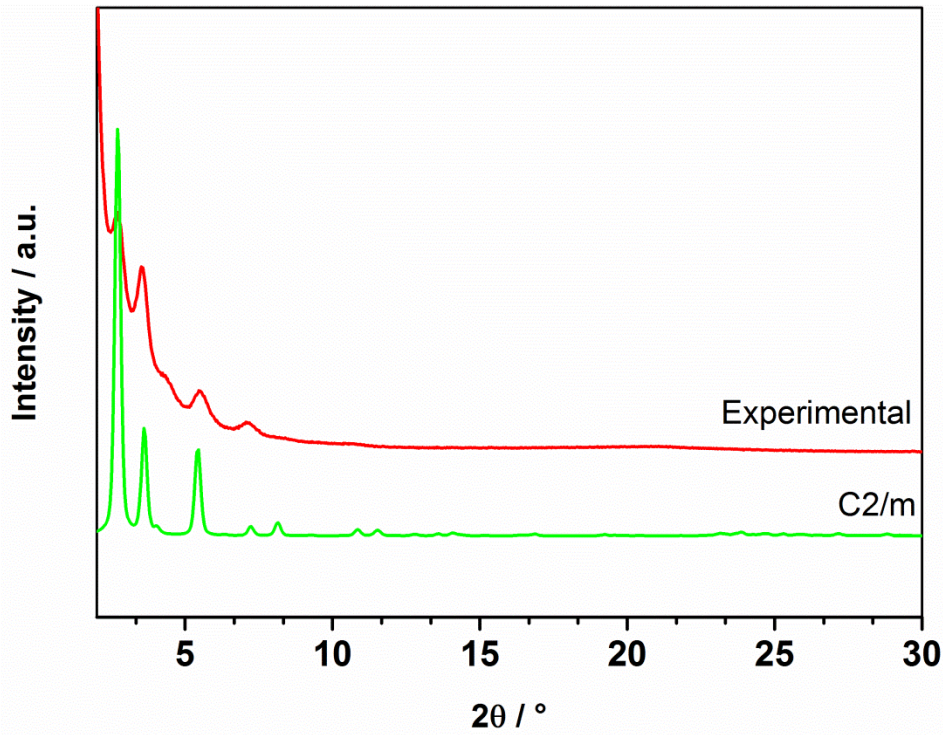

Figure S8. Powder XRD patterns of experimental data of **DPP-TAPP-COF** (red) simulated in the *C*2/*m* space group (green), respectively.

5 BET sorption measurements

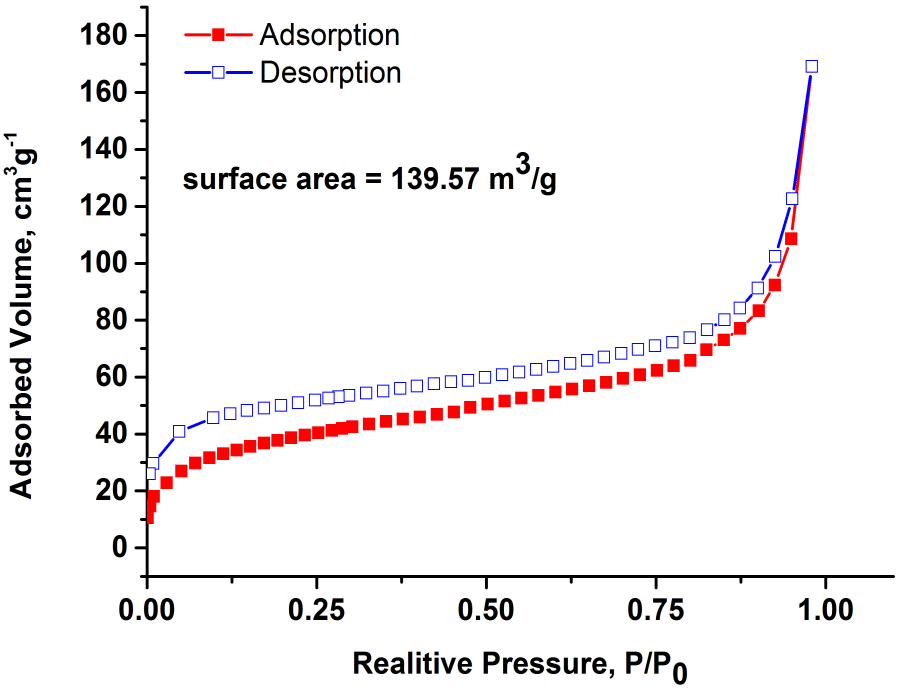

Figure S9. Nitrogen sorption isotherm of **DPP-TAPP-COF**. Full red symbols: adsorption, empty blue symbols: desorption.

6 Energy-dispersive X-ray spectroscopy (EDX)

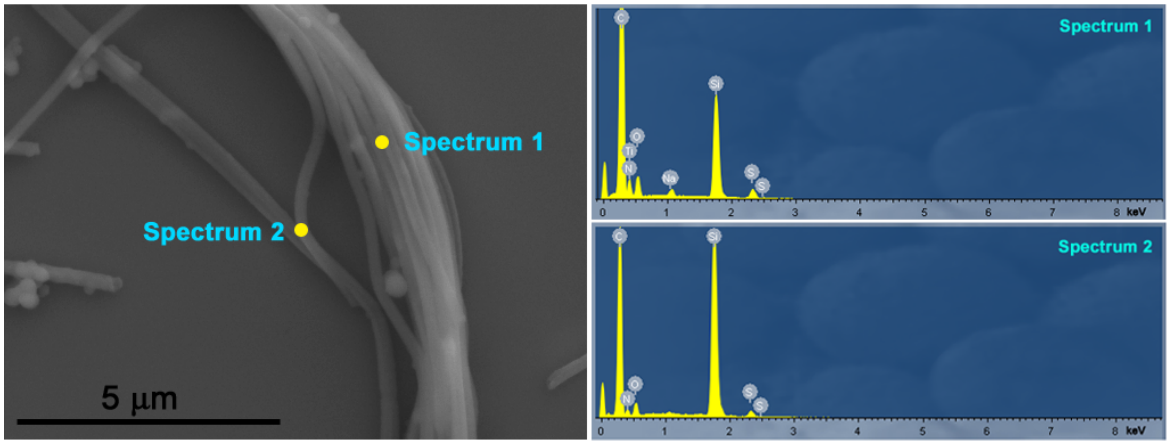

Figure S10. EDX mapping of the nanotubes at specific points indicating the elemental composition of C, N, O and S.

7 pH-dependent synthetic studies

In order to get deeper insights into the mechanism of the tube formation, pH-dependent synthetic studies were performed and analyzed by SEM. Under optimized conditions, hollow nanotubes could be reproducibly obtained using AcOH as catalyst in 0.15 molar concentration. Interestingly, at lower catalyst concentrations (0.05 M), spherical particles were obtained instead (Figure S11a and S11b). Reaction at slightly higher catalyst concentration (0.1 M) resulted in rod-like aggregates of similar spheres (Figure S11c and S11d). However, PXRD clearly revealed the predominantly amorphous character of these structures (Figure S14), and both STEM (Figure S12) and focused ion beam (FIB) microscopy (Figure S13) indicated that neither the spherical particles nor the rod-like aggregates are hollow structures but rather solid agglomerates. Therefore, it can be concluded that these particles are most likely not on-pathway intermediates towards the formation of the hollow microtubes but rather form via other pH-dependent pathways.

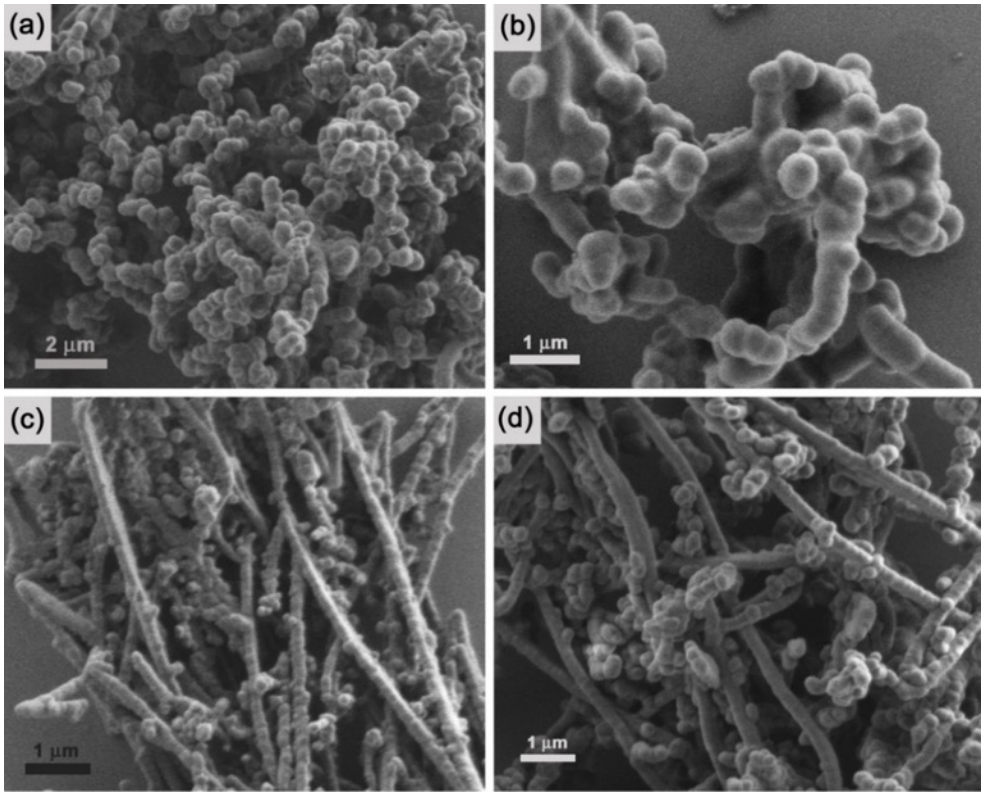

Figure S11. SEM micrographs of COF nanostructures obtained at different concentrations of AcOH as catalyst: (a) and (b) Spherical nanostructures obtained with 0.05 mol L^{-1} AcOH; (c) and (d) agglomeration of spherical nanostructures into rod-like aggregates with 0.1 mol L^{-1} AcOH.

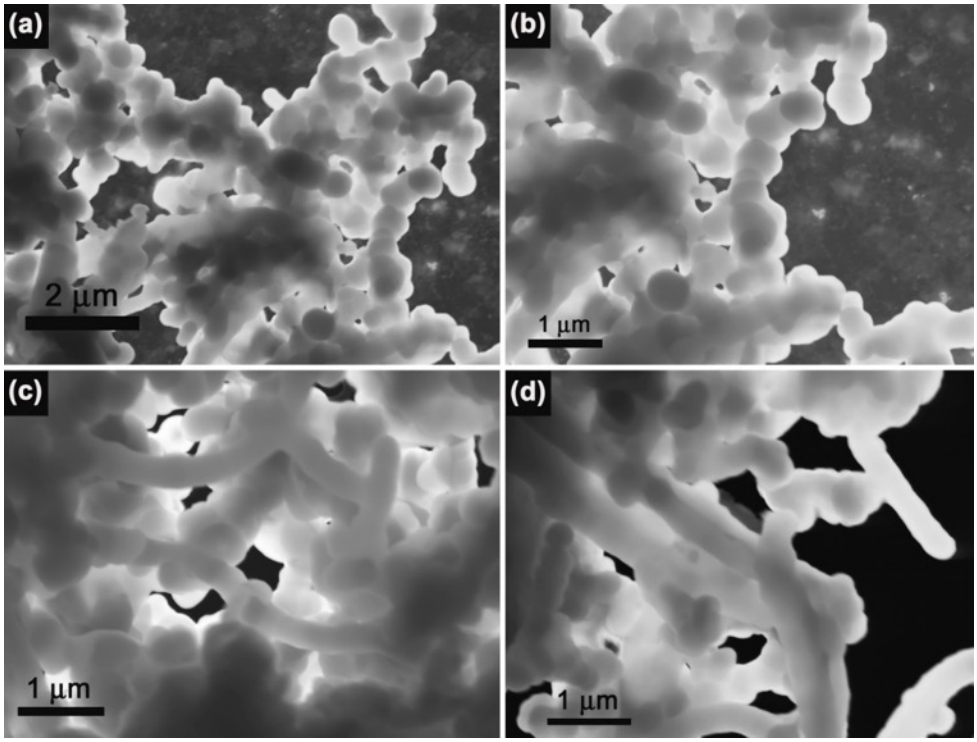

Figure S12. (a) and (b) STEM images of spherical particles obtained with 0.05 mol L^{-1} AcOH; (c) and (d) STEM images of rod-like aggregates obtained with 0.1 mol L^{-1} AcOH. All images indicate the solid nature of both nanostructures and exclude the formation of hollow structures.

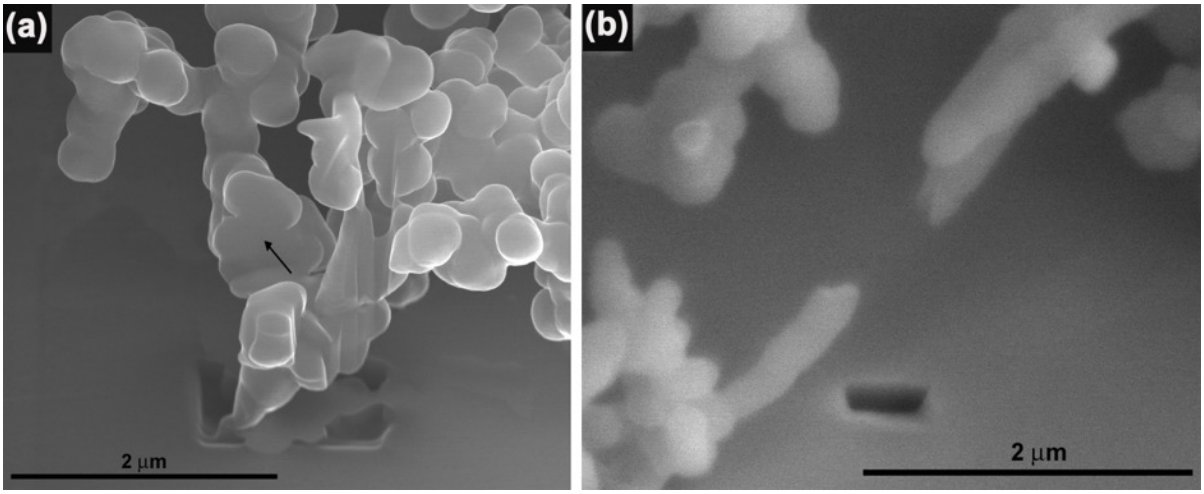

Figure S13. FIB experiments showing the solid nature and absence of hollow structures for (a) spherical particles obtained with 0.05 mol L^{-1} AcOH, and (b) rod-like aggregates obtained with 0.1 mol L^{-1} AcOH.

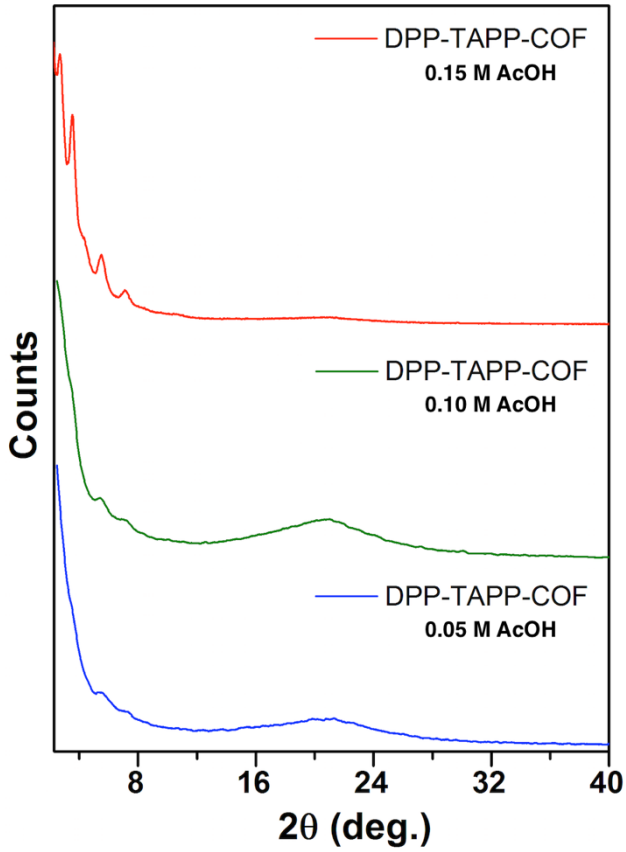

Figure S14. PXRD patterns for **DPP-TAPP-COF** synthesized in *n*-BuOH/mesitylene 3:1 at 120 °C with different concentrations of AcOH as catalyst.

8 Atomic force microscopy (AFM)

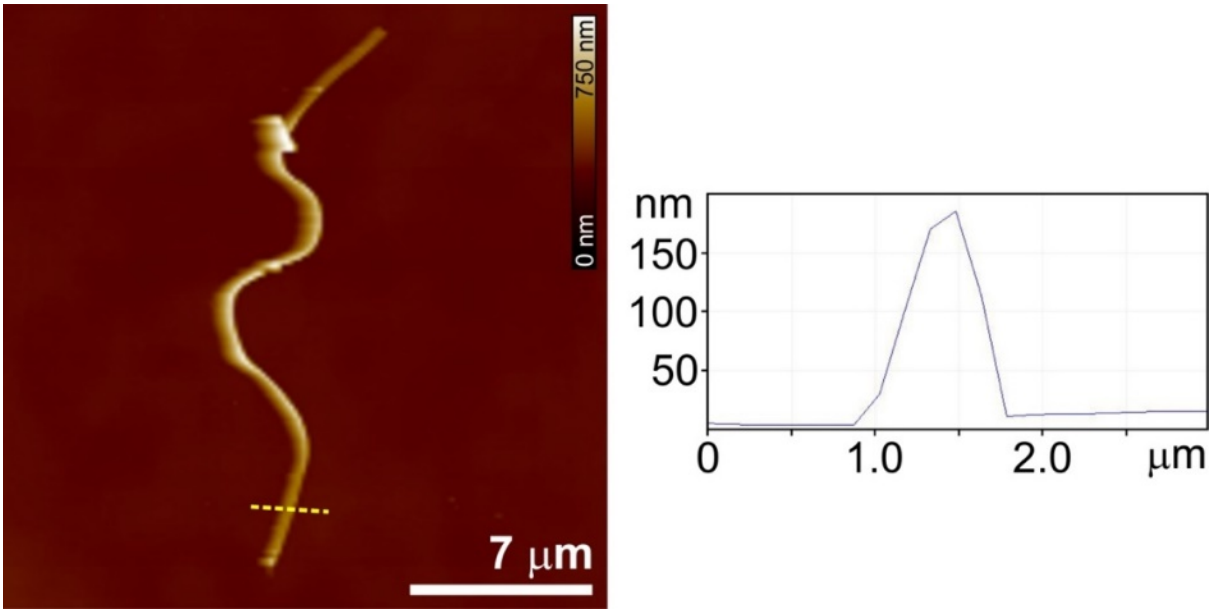

Figure S15. AFM image of one single nanotube together with its cross sectional height.

9 Time-dependent COF synthesis

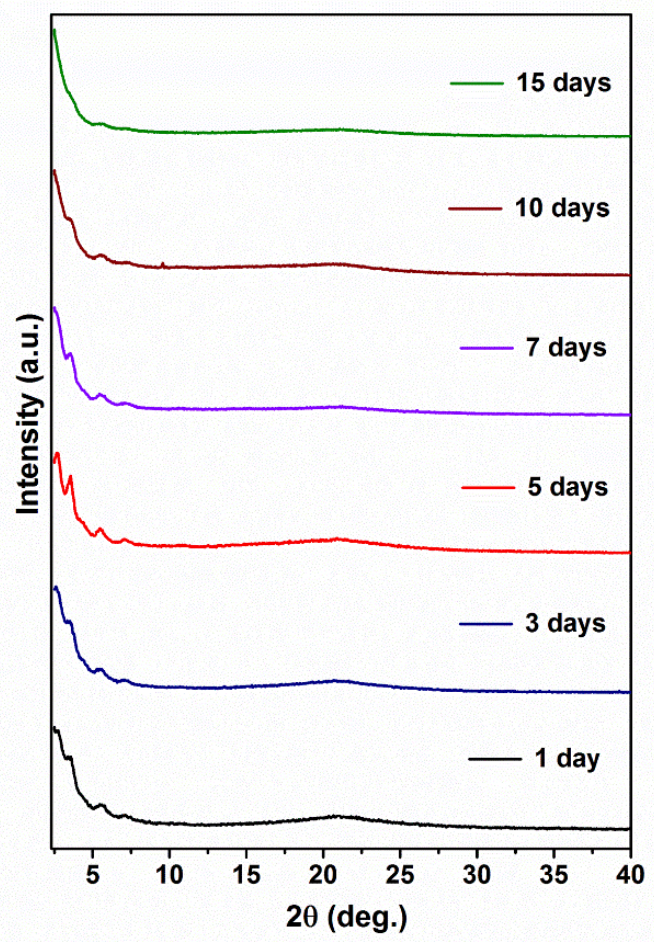

Figure S16. PXRD patterns for **DPP-TAPP-COF** synthesized in *n*-BuOH/mesitylene 3:1 at 120 °C; reaction was quenched after different time intervals as indicated.

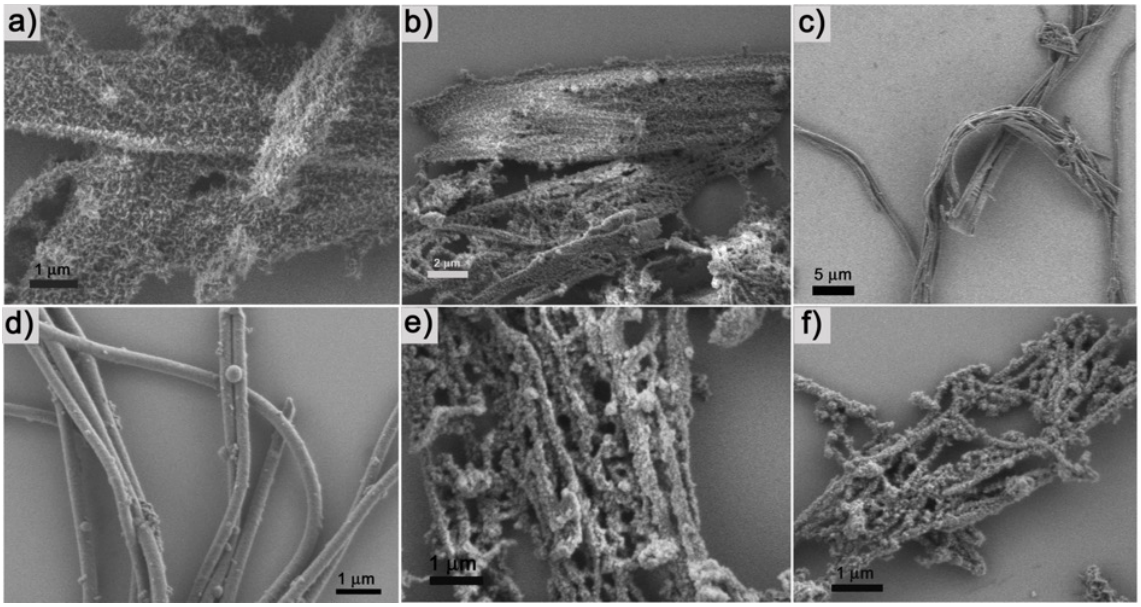

Figure S17. SEM micrographs of **DPP-TAPP-COF** synthesized in *n*BuOH/mesitylene 3:1 at 120 °C; reaction was quenched after a) one day, b) three days, c) four days, d) five days, e) seven days and f) ten days.

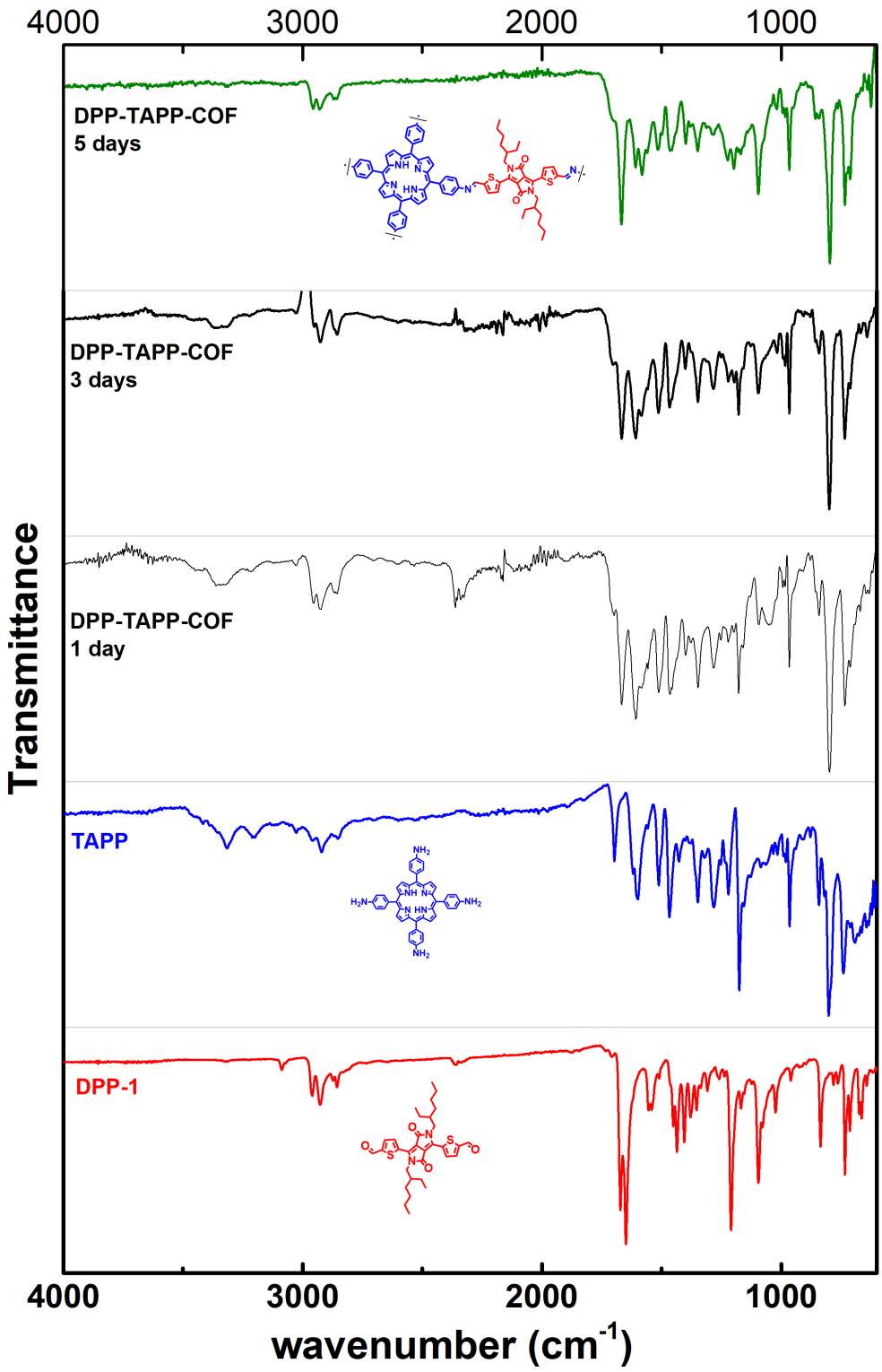

Figure S18. FTIR spectra for **DPP-TAPP-COF** (green), COF reactions quenched after one and three days (black) in comparison with monomers **TAPP** (blue) and **DPP-1** (red).

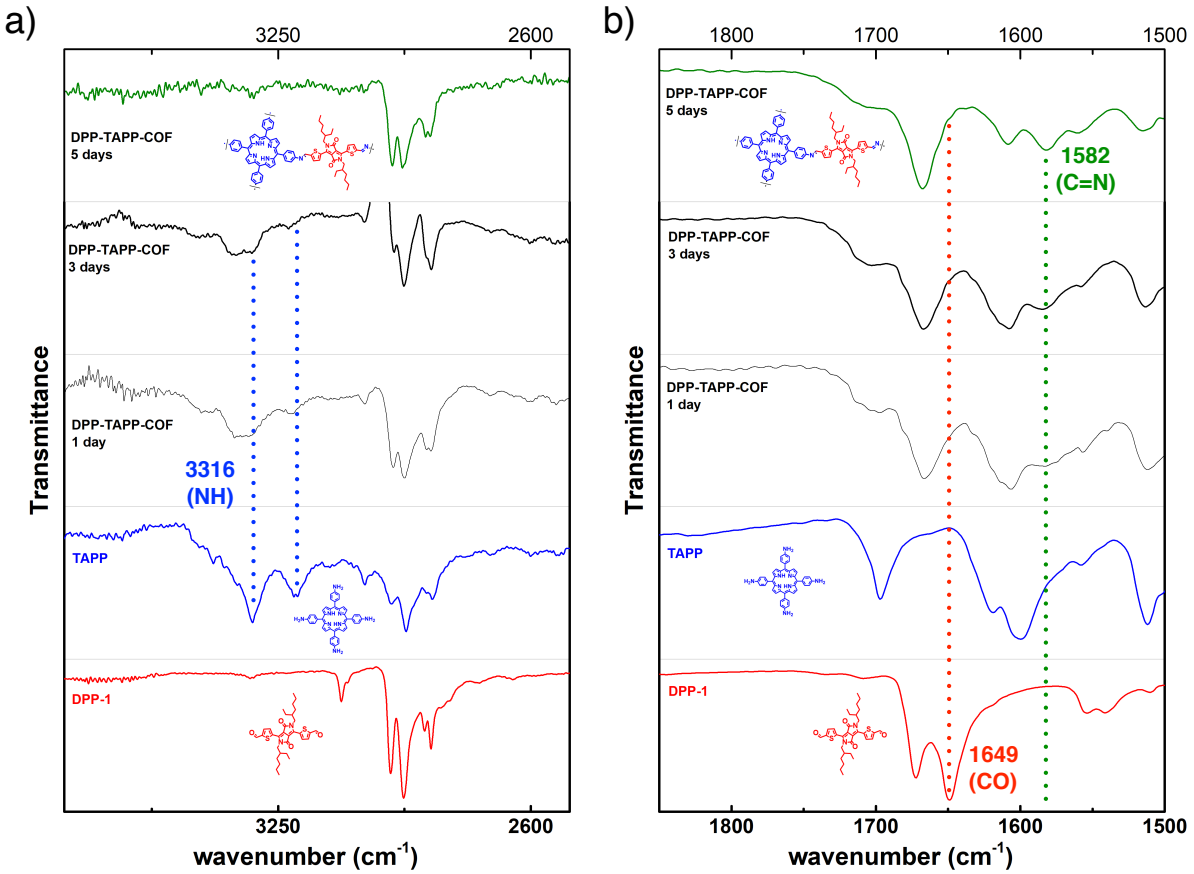

Figure S19. sections of FTIR spectra for **DPP-TAPP-COF** (green), COF reactions quenched after one and three days (black), **TAPP** (blue) and **DPP-1** (red) highlighting characteristic regions for a) NH stretching bands and b) C=O and N=H stretching bands.

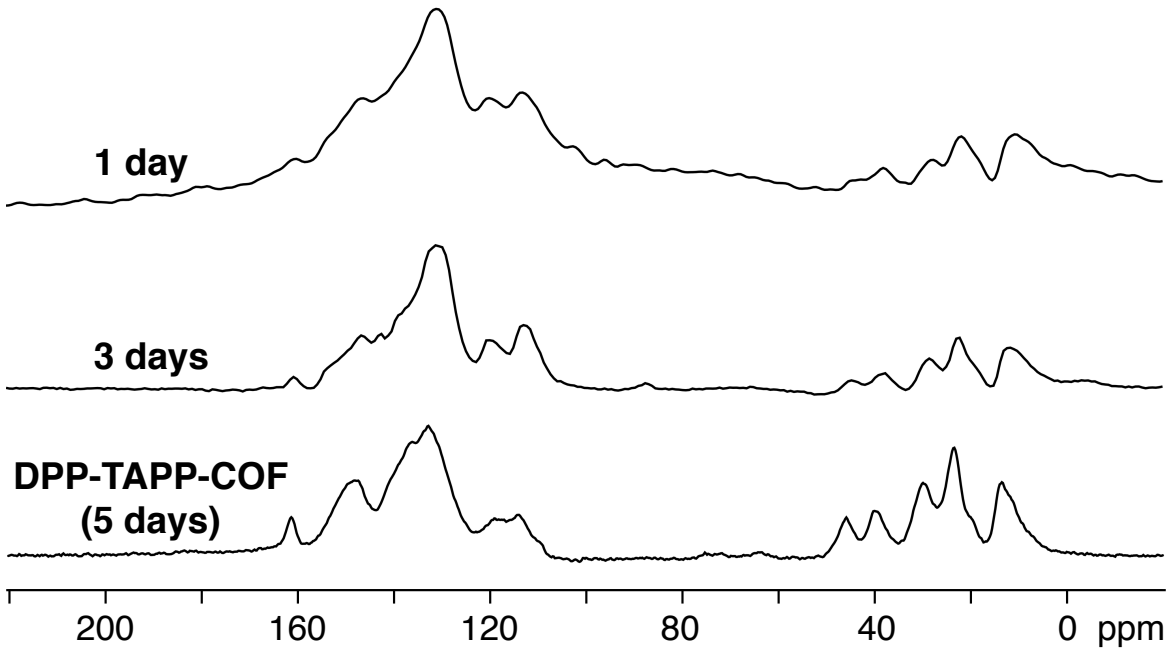

Figure S20. 13C-CP-MAS-NMR spectra of **DPP-TAPP-COF** reactions quenched after one (100.6 MHz, 13.5 kHz spin rate, top), three (100.6 MHz, 13.5 kHz spin rate, middle) and five days (151.0 MHz, 17.0 kHz spin rate, bottom, optimized reaction conditions).

10 Microscopic images and powder X-ray diffraction (PXRD)

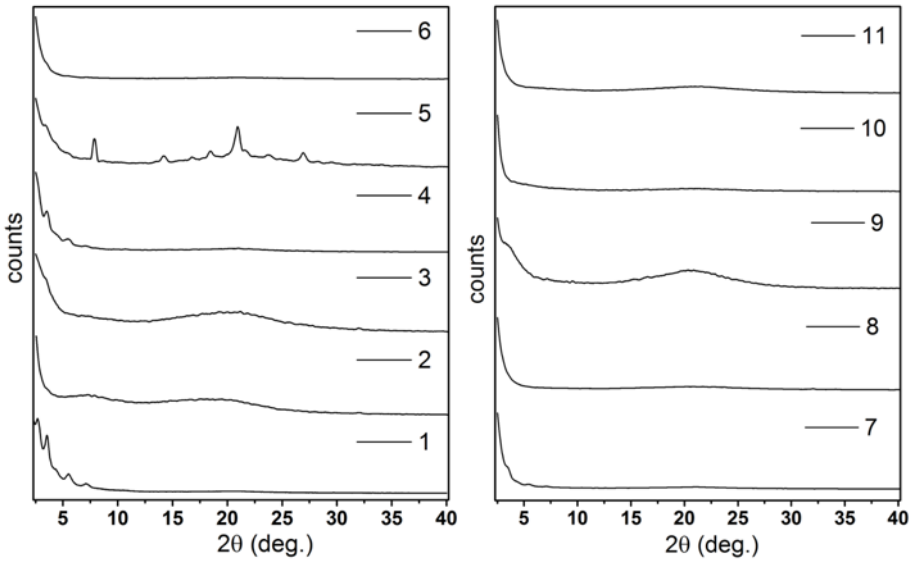

Figure S21. PXRD patterns for **DPP-TAPP-COF** synthesis in different solvents. Numbers indicate different entries of table S1.

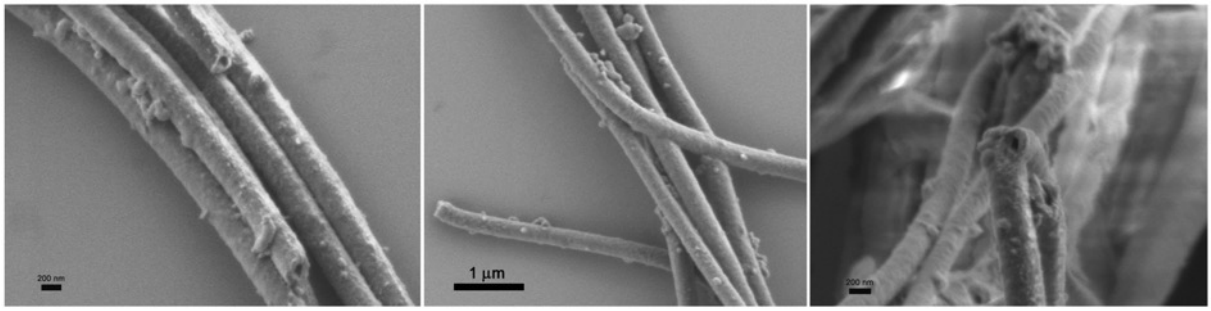

Figure S22. SEM micrographs of **DPP-TAPP-COF** nanotubes on different length scales.

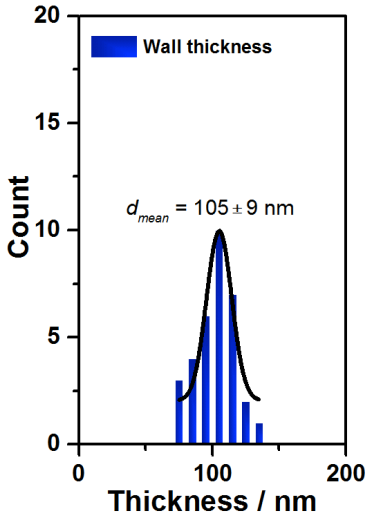

Figure S23. Statistical distribution of wall thickness for **DPP-TAPP-COF** nanotubes obtained from STEM micrographs.

11 References

[S1] L. Huo, J. Hou, H.-Y. Chen, S. Zhang, Y. Jiang, T. L. Chen, Y. Yang, *Macromolecules* **2009**, *42*, 6564–6571.

[S2] S. Meng, Z. Xu, G. Hong, L. Zhao, Z. Zhao, J. Guo, H. Ji, T. Liu, *Eur. J. Med. Chem.* **2015**, *92*, 35–48.

[S3] W. S. Yoon, S. K. Park, I. Cho, J.-A. Oh, J. H. Kim, S. Y. Park, *Adv. Funct. Mater.* **2013**, *23*, 3519–3524.

[S4] B. P. Karsten, R. K. M. Bouwer, J. C. Hummelen, R. M.Williams, R. A. J. Janssen, *Photochem. Photobiol. Sci.* **2010**, *9*, 1055–1065.

[S5] B. P. Karsten, J. C. Bijleveld, R. A. J. Janssen, *Macromol. Rapid Commun.* **2010**, *31*, 1554–1559.

[S6] R. Luguya, L. Jaquinod, F. R. Fronczek, M. G. H. Vicente, K. M. Smith, *Tetrahedron* **2004**, *60*, 2757–2763.

[S7] K. Ladomenou, T. Lazarides, M. K. Panda, G. Charalambidis, D. Daphnomili, A. G. Coutsolelos, *Inorg. Chem.* **2012**, *51*, 10548–10556.